HHS Public Access

Author manuscript

*Biomaterials*. Author manuscript; available in PMC 2019 October 01.

Published in final edited form as:

*Biomaterials*. 2018 October ; 179: 29–45. doi:10.1016/j.biomaterials.2018.06.032.

# Settable Polymer/Ceramic Composite Bone Grafts Stabilize Weight-Bearing Tibial Plateau Slot Defects and Integrate with Host Bone in an Ovine Model

**Sichang Lu**[1], **Madison AP McGough**[2], **Stefanie M Shiels**[3], **Katarzyna J Zienkiewicz**[1], **Alyssa R Merkel**[4,5], **Joseph P Vanderburgh**[1], **Jeffry S Nyman**[4,6], **Julie A Sterling**[4,5], **David J Tennent**[3], **Joseph C Wenke**[3], and **Scott A Guelcher**[1,2,4]

[1]Department of Chemical and Biomolecular Engineering, Vanderbilt University, Nashville, TN 37235

[2]Department of Biomedical Engineering, Vanderbilt University, Nashville, TN 37235

[3]Extremity Trauma and Regenerative Medicine Task Area, U.S. Army Institute of Surgical Research, Fort Sam Houston, TX

[4]Center for Bone Biology, Department of Medicine, Vanderbilt University Medical Center, Nashville, TN 37235

[5]Department of Veterans Affairs, Nashville, TN

[6]Department of Orthopedic Surgery and Rehabilitation, Vanderbilt University Medical Center, Nashville, TN 37235

## Abstract

Bone fractures at weight-bearing sites are challenging to treat due to the difficulty in maintaining articular congruency. An ideal biomaterial for fracture repair near articulating joints sets rapidly after implantation, stabilizes the fracture with minimal rigid implants, stimulates new bone formation, and remodels at a rate that maintains osseous integrity. Consequently, the design of biomaterials that mechanically stabilize fractures while remodeling to form new bone is an unmet challenge in bone tissue engineering. In this study, we investigated remodeling of resorbable bone cements in a stringent model of mechanically loaded tibial plateau defects in sheep. Nanocrystalline hydroxyapatite-poly(ester urethane) (nHA-PEUR) hybrid polymers were augmented with either ceramic granules (85% β-tricalcium phosphate/15% hydroxyapatite, CG) or a blend of CG and bioactive glass (BG) particles to form a settable bone cement. The initial compressive strength and fatigue properties of the cements were comparable to those of non-resorbable poly(methyl methacrylate) bone cement. In animals that tolerated the initial few weeks of early weight-bearing, CG/nHA-PEUR cements mechanically stabilized the tibial plateau defects

**Data Availability Statement**

The raw and processed data required to reproduce these findings cannot be shared at this time due to technical or time limitations.

and remodeled to form new bone at 16 weeks. In contrast, cements incorporating BG particles resorbed with fibrous tissue filling the defect. Furthermore, CG/nHA-PEUR cements remodeled significantly faster at the full weight-bearing tibial plateau site compared to the mechanically protected femoral condyle site in the same animal. These findings are the first to report a settable bone cement that remodels to form new bone while providing mechanical stability in a stringent large animal model of weight-bearing bone defects near an articulating joint.

### Keywords

bone cement; weight bearing fracture; tibial fracture; nanocrystalline hydroxyapatite

## Introduction

Intra-articular fractures frequently involve a weight-bearing joint and often require internal fixation with subchondral grafting to maintain articular congruence.[1, 2] The use of calcium phosphate cements (CPCs) with buttress plating mitigates the loss of reduction[3], but the use of large internal fixation devices can increase complications.[4] Patients' non-compliance with limiting weight-bearing activities for 10 weeks also increases complications.[5] Consequently, up to 25% of severe tibial plateau fractures fail and require rehospitalization[5], resulting in increased risk of a poor outcome at 2 years post-injury.[6]

An ideal grafting material for treatment of intra-articular fractures would: (i) set within minutes after implantation in the defect, (ii) rapidly provide bone-like strength to stabilize the defect and maintain articular congruence with minimal use of hardware to support fixation, (iii) stimulate new bone formation, and (iv) resorb at a rate aligned with patient biology to maintain osseous integrity as the graft is gradually replaced by bone. Poly(methyl methacrylate) (PMMA) bone cements are indicated for structural repair of bone due to their high strength (70 – 90 MPa), but they are non-resorbable, do not integrate with host bone[7–11], and are not suitable for treatment of tibial plateau fractures. Biomaterials that mechanically stabilize intra-articular fractures while remodeling to form new bone are not currently available and thus represent a long-standing unmet need in bone tissue engineering.

CPCs have been shown to be osteoconductive and resorbable *in vivo*.[2, 12–18] In an early study, a carbonated apatite cement mechanically stabilized weight-bearing tibial plateau slot defects in 25-kg mongrel dogs while slowly undergoing osteoclast-osteoblast coupled creeping substitution over a period of 72 weeks.[19] At 16 weeks, resorption of the cement was slightly faster in mechanically loaded tibial plateau defects (78% of the cement remaining) compared to mechanically protected femoral condyle defects (85% of the cement remaining). However, when implanted in mechanically loaded tibial plateau defects in 50-kg sheep, there were gaps between carbonated apatite cement and the host bone, cracks within the cement, and fractures in the tibial plateau.[20] Also in this study, a biphasic cement comprising a fast-resorbing dicalcium phosphate dehydrate (DCPD) matrix filled with slow-resorbing β-tricalcium phosphate (β-TCP) granules remodeled faster than the carbonated

apatite cement but showed similar cracking and resorption gaps. Consequently, CPCs are indicated for use as bone void fillers and not for structural repair of bone.[20]

Injectable, settable, and resorbable biphasic poly(ester urethane) (PEUR) composite bone grafts exhibit working times comparable to CPCs, support bone remodeling, and degrade to nontoxic compounds.[21–26] However, the mechanical properties of these composites are limited by the low strength of PEUR.[27, 28] In a recent study, lysine triisocyanate (LTI) was grafted to nanocrystalline hydroxyapatite (nHA) particles and crosslinked with poly(ε-caprolactone) triol to create nHA-PEUR hybrid inorganic-organic polymers with bending and compressive strengths >90 MPa, which is sufficiently high to support structural repair of bone.[29] nHA-PEUR stimulated osteoid mineralization and exhibited osteoclast-mediated resorption *in vitro*[29] and *in vivo*.[30] These nHA-PEUR hybrid polymers are resistant to hydrolytic degradation (<2% mass loss after 4 months at 37¼C *in vitro*)[31, 32] but readily degrade in the presence of reactive oxygen species (ROS) secreted by infiltrating cells.[32, 33] Thus, nHA-PEUR-derived bone cements are anticipated to provide mechanical stability as they remodel, since they undergo negligible degradation until cells infiltrate the cement. While these biomaterials meet the criteria of bone-like strength, stimulation of osteogenic differentiation, and resorption by osteoclasts, their ability to promote bone healing of weight-bearing fractures has not been previously investigated.

In the present study, we hypothesized that biphasic ceramic/nHA-PEUR composite bone cements would maintain stability of mechanically loaded tibial plateau defects while remodeling to form new bone. The nHA-PEUR polymer was augmented with ceramic particles to yield settable cements with handling properties comparable to conventional bone cements. Two types of ceramic particles were tested: slow-resorbing ceramic mini-granules (CG, 85% β-tricalcium phosphate/15% hydroxyapatite) and fast-resorbing 45S5 bioactive glass (BG) particles. Biphasic cements were implanted in mechanically loaded tibial plateau slot defects in sheep. Previous studies have reported that currently available bone cements have failed in this mechanically stringent model.[20] Ceramic/nHA-PEUR cements were also implanted in mechanically protected femoral condyle plug defects in the same animal [20] to investigate the effects of ceramic composition and mechanical loading on remodeling of the implants.

## Materials and Methods

### Materials

Lysine triisocyanate (LTI) was purchased from Jinan Haohua Industry Co., Ltd (Jinan, China) and purified by refluxing with activated carbon (Fisher Scientific) in *t*-butyl methyl ether (TBME, Across-Organic) at 63°C for 22 hours before use. Poly(ε-caprolactone) (PCL) triol ($M_n$ = 300 Da) and nHA particles were purchased from Sigma-Aldrich and dried under vacuum at 80°C for 48 hours before use. Iron acetylacetonate (FeAA) catalyst, 3-amino-propyl-triethoxysilane (APTES), and ε-caprolactone were purchased from Sigma-Aldrich and used as received. Magnesium sulfate and stannous octoate ($Sn(Oct)_2$) were purchased from Thermo Fisher Scientific. Melt-derived 45S5 bioactive glass (BG) was purchased from Mo-Sci Corporation (Rolla, MO). Slow-resorbing ceramic granules (CG, 85% β-tricalcium phosphate / 15% hydroxyapatite) were supplied by Medtronic (Memphis, TN) and ground to

100–300 μm diameter using a mortar and pestle. BG and CG particles were cleaned by sonicating with 95% acetone for 5 minutes, triple rinsed with DI water, and vacuum dried before use. CD31 antibody (NB 100-65900, Novus Biologicals, Littleton, CO), endomucin antibody (LS-C383339-100, LifeSpan BioSciences, Inc., Seattle, WA), and secondary antibodies (C-2764 and A-31574, ThermoFisher Scientific) were diluted according to manufacturers' recommendations for immunofluorescence staining. Immunohistochemical staining was performed using anti-sclerostin primary antibody (ab63097 AbCam) and goat anti rabbit-HRP secondary antibody (sc-2004 SantaCruz) diluted as recommended by the manufacturers. A NovaRed Chromagen Kit and hematoxylin stain were purchased from SK-4805 Vector Laboratories and Fisher Scientific, respectively.

### Surface-initiated polymerization of ε-caprolactone on BG

We have previously shown that grafting PCL to non-porous BG particles significantly enhances the strength and fatigue properties of BG/PEUR composites due to increased interfacial bonding between the BG and PEUR phases.[34] The method for surface-initiated polymerization of ε-caprolactone on BG has been described previously.[35] Briefly, clean BG particles were stirred in APTES solution (2 μM in 9:1 (v/v) ethanol:DI water) for 5 hours at room temperature, followed by annealing at 100°C for 1 h. Before polymerization, ε-caprolactone was dried in the presence of magnesium sulfate. Silanized BG particles were reacted with a mixture comprising 0.001M $Sn(Oct)_2$ in dried ε-caprolactone at weight ratio of 1:3.679 at 110°C for 24 hours. The PCL-grafted BG particles were extracted, washed with chloroform, and dried at 40°C under vacuum. Grafted BG particles contained 0.16 wt% PCL as measured by TGA.[35]

### Synthesis of nHA-LTI prepolymer

nHA-LTI prepolymer was synthesized by mixing nHA particles (65 wt%) with LTI (35 wt %) in the presence of FeAA catalyst (5% solution in ε-caprolactone, overall 0.55 wt%) at weight ratio of 1:0.0055 for 10 minutes and maintained at 50°C for 3 hours to yield a viscous liquid.[29]

### Synthesis of polymer/ceramic composite bone grafts

nHA-LTI prepolymer crosslinked with PCL triol yields a tacky nHA-PEUR polymer that can be injected but not handled as a putty prior to cure.[32] The reactive nHA-PEUR polymer (54 wt% nHA) was augmented with CG or a mixture of CG and BG to yield a putty that could be implanted by hand into the defects. Polymer/ceramic composite bone grafts were made by first mixing PCL triol ($M_n$ = 300 Da) with FeAA catalyst (5% solution in ε-caprolactone, overall 0.44 wt% FeAA in PCL triol) until homogenous. The PCL triol/FeAA mixture was then mixed with CG (55 wt%) or a blend of BG (37.5 wt%) and CG (22.5 wt%) particles until the surface of the particles was uniformly covered by PCL triol/FeAA. The amount of CG and BG in the blend was designed to achieve a 1:1 volume ratio of CG:BG. Finally, the PCL triol/FeAA/CG and PCL triol/FeAA/BGCG pastes were reacted with nHA-LTI prepolymer by hand-mixing for another 30 s. The ratio of isocyanate (NCO):hydroxyl (OH) equivalents was 1.4:1. The resulting composite bone grafts were denoted as CG/nHA-PEUR and BGCG/nHA-PEUR. The CG/nHA-PEUR cement incorporated 55 wt% CG, 24.3

wt% nHA, and 20.7 wt% PEUR, and the BGCG/nHA-PEUR cement incorporated 37.5 wt% BG, 22.5 wt% CG, 21.6 wt% nHA, and 18.4 wt% PEUR.

### In vitro characterization of ceramic/nHA-PEUR composite bone grafts

Thirty seconds of mixing yielded a moldable cement that can be conformed to the defect space prior to *in situ* cure. Working time was determined as the time at which the grafts could no longer be compressed, and tack-free time was measured as the time at which a metal spatula no longer stuck to the graft. The tack-free time approximates the setting time for bone cements.[36]

### Compressive mechanical properties

Cylindrical specimens were used for all mechanical testing. Composites were mixed as described above, cured in a 6-mm diameter tube under a 1.0-kg weight for 24 hours[37], and cut to a height of 12 mm using a Buehler IsoMet Low Speed Saw to maintain parallel surfaces. Specimens were hydrated in water for 24 h at 37 °C prior to quasi-static compressive testing. Hydrated specimens were compressed at a rate of 25 mm $min^{-1}$ using an MTS 858 Bionix Servohydraulic Test System. Compressive modulus, yield strength, and yield strain were calculated from the resulting engineering stress-strain curve (n = 7 for CG/nHA-PEUR and n = 8 for BGCG/nHA-PEUR). The yield point (intersection between the dashed line and the CG curve in Figure 1A) was calculated based on the 0.2% offset method, and the ultimate point (intersection between the solid line and the CG curve in Figure 1A) was defined as the maximum stress. The compressive failure point (intersection between the dotted line and the CG curve in Figure 1A) was defined as the first inflection point after softening (drop in compressive stress after reaching the ultimate point). The post-yield strain was defined as the additional strain after yielding required to reach material failure. The stress-strain curve was divided into the three zones shown in Figure 1A: (1) elastic zone (from the initial to the yield point), (2) post-yield zone (from the yield to the ultimate point), and (3) fracture zone (from the ultimate to the failure point).[38] The energy absorbed by the composite in each of these zones was calculated as the area under the curve of the corresponding zone. The modulus of resilience represents the elastic energy absorbed (zone 1), while the post-yield toughness (zone 2) and fracture zone toughness (zone 3) represent the energy absorbed during plastic deformation and are a measure of ductility.

Fatigue testing was performed as described previously (n = 3).[26] The linear actuator was equipped with cylindrical platens having a diameter only slightly larger than the specimen. After loading the hydrated specimen with ~1 N force, an MTS extensometer (634.31F-24) was attached to both platens. Hydration was maintained throughout the testing by a constant water drip supplied from a water bath heated to 37 °C. Fatigue properties were assessed by cyclically loading specimens to a maximum stress of 5 MPa (minimum ~0.3 MPa to maintain contact) at a frequency of 5 Hz. The same proportional and integral terms were used for the entire group. Force and strain were recorded for every $500^{th}$ cycle at an acquisition frequency of 200 Hz. Testing was stopped when runout ($10^6$ cycles) or greater than 3.5% strain was reached. Compressive fatigue failure was defined by either 1% creep deformation or 3% increase in strain. Creep deformation was measured by comparing the minimum strain value of each cycle to that of the initial cycle recorded.

### In vivo sheep study

This study was approved by the Institutional Animal Care and Use Committee of the US Army Institute of Surgical Research and conducted in compliance with the Animal Welfare Act, the implementing Animal Welfare Regulations, and the principles of the Guide for the Care and Use of Laboratory Animals. Eight skeletally mature (4-years old) female Rambouillet sheep weighing 54.9 + 4.3kg were used for the *in vivo* animal study. Animals received glycopyrrolate (0.01mg/kg, SC) approximately 1 hour prior to surgery and were premedicated with carprofen (2mg/kg SC) and a caudal epidural injection of morphine (0.1mg/kg). Anesthesia was induced with a combination of ketamine hydrochloride (2.75mg/kg) and medazolam (0.25mg/kg) given intravenously and a surgical plane of anesthesia maintained with 1–3% isoflurane via endotracheal intubation. With fluoroscopic guidance, two types of bony defects were prepared in each posterior extremity: a non-weight-bearing femoral plug defect (n = 16 per treatment group) and a weight-bearing tibial plateau slot defect (n = 8 per treatment group). Two non-weight-bearing plug defects, with a 6 mm diameter and a 16 mm depth, were created on the medial and lateral distal condyles of both femurs. This defect size has been reported as suitable for evaluating bone regeneration in sheep.[39] A single weight-bearing tibial plateau slot defect was created proximal to the patella tendon insertion and approximately 3 mm distal to the tibial plateau articular surface as described previously.[20] A load of 1.21 ± 0.24 kN, which corresponds to approximately two times the weight of the sheep and occurs during its normal gait, has been reported to be sufficient to fracture the plateau if the defect is not grafted.[40] The defects encompassed the entire medial to lateral width, had a depth that was approximately 50% of the total anterior to posterior tibial depth, and were 6 mm high. Each of the defects was filled with one of two grafts, BGCG/nHA-PEUR or CG/nHA-PEUR, by hand-packing the cement into the defect. Each sheep received both grafts in separate extremities, and the placement of grafts was alternated between animals. For example, one sheep had BGCG/nHA-PEUR grafts in the left posterior extremity and CG/nHA-PEUR grafts in the right posterior extremity, and the other one had BGCG/nHA-PEUR in the right and CG/nHA-PEUR in the left. The animals were recovered and placed in a sling for 3 days post-operatively before allowing full weight-bearing as tolerated. Animals received slow-release buprenorphine (10mg/kg IM) immediately postoperatively and as needed for breakthrough pain. Immediately after surgery and at 4, 8, 12, and 16 weeks, animals were sedated and imaged using computed tomography (CT, Prime Aquilon, Toshiba, Tokyo, Japan) at a resolution of 0.5 mm. Animals were sedated and euthanized at 16 weeks and femurs and tibias were harvested and placed in 10% neutral buffered formalin.

### Micro-computed tomography (μCT)

Specimens were loaded into 48-mm diameter tubes filled with 10% formalin and scanned using a μCT50 (SCANCO Medical, Bassersdorf, Switzerland). Micro-computed tomography (μCT) was performed with isotropic voxel size of 24.2 μm for qualitative analysis. For the tibial plateau and one of the femoral condyle defects in each limb, Scanco software was used to contour an area from the host bone-implant interface (excluding residual implant) to 2 mm away from the defect. Four femoral condyle and four tibial plateau defects (two from each group) were not included in the analysis due to tibial plateau fractures at 2 – 3 weeks. However, defects from the contralateral limbs that did not fracture were included in the

analysis, considering a previous study reporting trabecular thickening near implanted bone grafts as early as 2 weeks.[23] Thus, n = 6 for the BGCG/nHA-PEUR and CG/nHA-PEUR groups at each anatomic site. The contour was subsequently segmented and morphed through 100 slices resulting in a representative volume of >100 $mm^3$ around the defect. The bone morphometric parameters in this interfacial region were analyzed in the Scanco software using a threshold setting of 240 mgHA/$cm^3$ and a sigma of 0.2 and support of 1 (Gaussian filter) to suppress noise. The same procedure was used to analyze the distant region (2 – 4 mm away from the defect), which was projected 2 mm radially from the outer edge of the initial contour (Figure 2E).

### Histology and histomorphometry

Sheep femurs and tibias were fixed in 10% formalin for 2 weeks, dehydrated in a series of ethanol solutions, and embedded in PMMA. An Exakt band saw was used to cut 200-μm sections (sagittal sections of tibias, transverse sections of femurs) from the center of the defects that were then ground (40–70 μm) and polished using an Exakt grinding system. The resulting sections were stained with Sanderson's Rapid Bone stain, counterstained with van Gieson, and imaged under a light microscope. For histomorphometric analysis, the defects were divided into rectangular areas of interest (AOI) with 1 mm height and widths one-half of the total depths of the defects as we have described previously (Figure 3).[37, 41] Each AOI was numbered from the center of the defects based on its distance from the mid-section. As shown in Figure 3, the outer AOIs 4 and -4, which lie 3 – 4 mm away from the center line, include both cement and host bone due to the irregular boundaries of the defect. Considering previous studies reporting densification of host bone surrounding the cement [37, 41], the reaction of the bone to the implanted cement was assessed in the interfacial AOIs 4 and −4. Area-% new bone, CG, and nHA-PEUR were measured for each region at early and late time points using Metamorph® software. For area-% CG and nHA-PEUR measurements, overexposed images were taken in order to distinguish them from the graft bulk.

### Immunofluorescence Staining

Polished sheep sections were washed with PBS and blocked with 5% goat serum in PBS for 1 h. CD 31 (1:50) and endomucin (1:500) primary antibodies were diluted in 5% goat serum and incubated with sections at room temperature for 2 h. The sections were then washed with TPBS and incubated in the dark with secondary antibodies (4 μg/ml) for 1 hour. Finally, sections were washed with TPBS and mounted with Aquamount. Stained sections were imaged using a Zeiss LSM 710 confocal microscope.

### Immunohistochemical staining

Polished sheep sections were washed with PBS with 0.1% Triton x-100 to permeabilize the membrane. Heat-mediated antigen retrieval was performed with citrate buffer at 80°C for 30 min. Samples were blocked in 5% goat serum for 1 h and incubated with anti-sclerostin antibody (1:25) overnight at 4°C followed by incubation in goat anti rabbit-HRP secondary antibody (1:500) for 1 h at room temperature. Sclerostin expression was detected with NovaRed Chromagen Kit following the manufacturer's directions. Samples were counterstained with hematoxylin and cover slipped with Aquamount. Stained sections were

imaged at 4x, 10x, 20x, and 40x magnification using an Olympus BX41 Microscope. Quantification of sclerostin staining in the sheep sections was performed on 4x images using thresholding and ROI analysis on Metamorph Image Analysis Software (Molecular Devices). A line to define the ROI was drawn around the trabeculae (excluding voids between trabeculae and bony surfaces to minimize artefacts) of the host bone adjacent to the graft approximately 3.5 mm deep. The area% sclerostin was calculated as the area stained positive for sclerostin divided by the total area.

### Dynamic histomorphometry

Animals intravenously received calcium-binding fluorochromes, which are deposited at sites of active mineralization and allow for sequential monitoring of new bone formation using histology.[42] Fluorochromes were given at the following time points: calcein green (10mg/kg) at 4 weeks, xylenol orange (80mg/kg) at 8 weeks, and oxytetracycline (20mg/kg) at 15 weeks. Sections were prepared as described above and imaged using a fluorescent microscope equipped with a DAPI/FITC/Texas Red filter (Chroma, Bellows Falls, VT).

### Statistical analysis

All data are plotted as the mean ± standard error of the mean (SEM). A Student t-test was applied to identify significant differences in mechanical properties between the BGCG/nHA-PEUR and CG/nHA-PEUR groups. A multiple ANOVA was applied to assess the significance of the effects of material composition, anatomic site, and proximity to the implant on the morphometric parameters of the host bone. For histomorphometry, a one-way ANOVA was performed for each AOI (−4 to 4) between the mechanically loaded tibial plateau and mechanically protected femoral condyle defects at 16 weeks. A one-way ANOVA was also performed for the CG/nHA-PEUR and BGCG/nHA-PEUR groups for each AOI on the distal surface (AOIs 1 to 4) between the sheep sacrificed at <3 weeks and 16 weeks.

## Results

### In vitro characterization of polymer/ceramic composite bone grafts

The working times for CG/nHA-PEUR grafts and BGCG/nHA-PEUR grafts were 2.08 ± 0.07 min and 2.26 ± 0.11 min, respectively (Table 1). For both groups, the tack-free time was equivalent to the working time, which suggests that the ceramic granules enhanced handling properties by reducing the tackiness of the settable polymer. Both groups hardened within 20 s after the working time, yielding a rigid cement that could not be compressed by hand.

Samples for mechanical testing were prepared by the same procedure and cured in cylindrical tubes for testing. Representative stress strain curves show the elastic (zone I), post-yield (zone II), and fracture (zone III) zones for the BGCG/nHA-PEUR and CG/nHA-PEUR groups (Figure 1A). The Young's modulus of the BGCG/nHA-PEUR group was significantly higher than that of the CG/nHA-PEUR group (Figure 1B), while the ultimate strength (Figure 1C), yield strength (Figure 1D), and stress softening (Table 2) were comparable for the two groups. However, the yield strain (Figure 1E), failure strain (Figure

1F), strain at ultimate strength (Table 2), and post-yield strain (Table 2) were significantly lower for BGCG/nHA-PEUR compared to CG/nHA-PEUR. Furthermore, CG/nHA-PEUR absorbed a greater amount of energy than BGCG/nHA-PEUR, as indicated by a significantly higher modulus of resilience (zone I), post-yield toughness (zone II), fracture zone toughness (zone 3), and overall toughness (zones I - III) (Table 2). These findings suggest that the addition of BG to the composites made the material more brittle.

The dynamic compression fatigue testing is illustrated schematically in Figure 4A–B. All specimens exceeded a runout of $10^6$ cycles of loading at a peak compressive stress of 5 MPa for both definitions of failure (1% creep deformation and 3% increase in strain). Representative hysteresis loops for the first (black) and last (gray) recorded cycle ($n$ = cycle number) are shown for CG/nHA-PEUR (Figure 4C) and BGCG/nHA-PEUR (Figure 4D) grafts. Creep strain at cycle $n$ (minimum strain of $n$th cycle – minimum strain of first recorded cycle) experienced by the grafts increased dramatically the first 50,000 cycles, but then reached a steady state as the tests progressed (Figure 4E–F). Neither group experienced greater than 0.25% creep up to 1,000,000 cycles, which confirms that the specimens did not fail before runout was reached. A slightly higher increase in creep strain at runout ($n$ = 1,000,000 cycles) for CG/nHA-PEUR (0.25%, Table 2) compared to BGCG/nHA-PEUR (0.14%) indicates accumulation of strain as the test proceeded.

## Pre-clinical outcomes

Representative CT images acquired immediately following the surgery show axial and sagittal views of tibial plateau and femoral plug defects filled with CG/nHA-PEUR (Figure 5A–C) and BGCG/nHA-PEUR (Figure 5D–G) grafts. Four of the eight sheep were sedated and euthanized early due to a combination of a ruptured patellar tendon and tibial shelf fractures near the upper surface of the defects in one of the posterior limbs. Of these, two sheep treated with BGCG/nHA-PEUR experienced ruptured tendons and fractures at 6 and 11 days, and two sheep treated with CG/nHA-PEUR experienced ruptured tendons and shelf fractures at 18 and 20 days (Table 3). However, it is not clear which of these events occurred first. Diagnostic CT (Supplemental Figure 1A) and μCT (Supplemental Figure 1B) images taken on the day of early sacrifice showed that one of the BGCG implants had fractured, while the others were intact. Additionally, two sheep visibly favored the CG/nHA-PEUR side immediately postoperatively, but their gait was improved after 3 weeks and the animals survived to 16 weeks. CT images of tibial plateau defects (Supplemental Figure 2) showed evidence of fragmentation of BGCG/nHA-PEUR grafts at 8, 12, and 16 weeks, while CG/nHA-PEUR grafts remained intact for the duration of the study.

## Histology analysis at early time points

The limbs of the sheep euthanized early (at 6 – 20 days) due to tibial plateau fractures were processed for histology (Figure 6). Among four CG/nHA-PEUR and four BGCG/nHA-PEUR tibial plateau explants, only one BGCG/nHA-PEUR explant showed significant material degradation (Supplemental Figure 1). The other seven grafts implanted in tibial plateau defects remained intact. In the femoral plug defects, all grafts remained intact for the duration of the study. Images of histological sections showed that the interface between the grafts and host bone was well-defined for both tibial plateau (Figure 6A, B) and femoral

plug defects (Figure 6E, F). While there was minimal incorporation of the graft with the host bone at this early stage, high magnification histology images of regions (shown in white boxes) near the host bone interface showed appositional bone growth near the interface (Figure 6C, D, G, H, stained red and labeled "B"). Residual nHA-PEUR (grayish brown regions labeled "P"), CG (black), and BG (transparent) were also evident in the high-magnification images. There were no resorption gaps or fibrous tissue observed in these defects.

### μCT at 16 weeks

At 16 weeks, BGCG/nHA-PEUR grafts implanted in tibial plateau defects degraded and fragmented (Figure 2A). There were large (>1 mm) gaps between the grafts and the host bone, and a rim of reactive new cortical bone appeared to be forming around the defect to compensate for the loss of mechanical stability caused by the rapid degradation of the grafts. In contrast, all 4 BGCG/nHA-PEUR grafts remained intact in femoral condyle defects at 16 weeks post-surgery and showed ingrowth of new trabeculae, suggesting that BGCG/nHA-PEUR grafts integrated with host bone (Figure 2B). CG/nHA-PEUR grafts were stable in both tibial plateau and femoral plug defects (Figure 2C–D). For the interface (adjacent to the implant) and the distant (far from the implant, Figure 2E) regions, the bone morphometric parameters BV/TV (Figure 2F), Tb.N. (Figure 2G), and Tb.Th. (Figure 2H) were measured. There were significant effects of proximity to the graft and anatomic site on BV/TV, Tb.N., and Tb.Th. The effects of implant composition were not significant and no significant two- or three-way interactions were observed. Consequently, pair-wise t-tests were performed to compare individual groups. Differences between adjacent and distant regions were significant for all BGCG/nHA-PEUR implants and for CG/nHA-PEUR tibial plateau implants. Differences in Tb.Th. between anatomic sites were significant for the BGCG/nHA-PEUR implants. For all other groups, morphometric parameters trended higher for the interface region and tibial plateau defects (Figure 2F–H).

### Histology at 16 weeks

Histological sections of the tibial plateau (Figure 7A, C, E) and femoral plug defects (Figure 7B, D, F) confirmed that the CG/nHA-PEUR grafts were stable. Images of histological sections of the tibial plateau defects near the host bone/graft interface showed structures similar to osteons (white circle) and Haversian canals (white arrow), which are the fundamental functional units of cortical bone (Figure 7C). Representative high-magnification images of interior regions of the tibial plateau (Figure 7E) and femoral plug (Figure 7F) defects showed ingrowth of new bone into the space between CG particles, which was formerly filled with nHA-PEUR, resulting in new bone growth on the surface of the CG particles. Multi-nucleated osteoclast-like cells were observed resorbing nHA-PEUR in the CG/PEUR group (Supplemental Figure 3A,C), and cellular infiltration was evident in histological sections of BGCG/PEUR (Supplemental Figure 3B,D). In contrast, BGCG/nHA-PEUR grafts fragmented in tibial plateau defects (Supplemental Figure 4A), and large resorption gaps filled with fibrous tissue and residual implant material were observed (Supplemental Figure 4C,E). Similar to the CG/nHA-PEUR group, structures appearing to be blood vessels were observed near the host bone/graft interface in tibial plateau defects (Supplemental Figure 4C). BGCG/nHA-PEUR grafts were stable in femoral plug defects

(Supplemental Figure 4B) and showed evidence of new bone and blood vessel formation (Supplemental Figure 4D, F).

A higher magnification confocal microscope image of a representative Haversian system is shown in Figure 8A. A ring of new bone labeled with xylenol orange deposited at 8 weeks (arrow, Figure 8B) was observed surrounding the Haversian canal. New bone labeled with calcein green deposited at 4 weeks was also observed (arrow, Figure 8C). Osteoblasts form lamellae sequentially from the external surface of an osteon inward toward the Haversian canal. The calcein green band deposited at 4 weeks is closer to the osteon than the xylenol orange band deposited at 8 weeks, indicating that the new bone formation observed in the lower right corner of Figure 8F was directed away from the osteon. Thus, the locations of the labeled bands suggest that this new bone formed independently of the osteon in the center. Immunofluorescence staining of endothelial markers CD31 (red staining, yellow arrow, Figure 8D) and endomucin (blue staining, yellow arrow, Figure 8E) revealed evidence of blood vessels in the new bone that formed after graft resorption. The images in Figures 8B, *C*, D, and E were merged in Figure 8F. Due to overlapping emission spectra between the xylenol orange (610 nm) and the Alexa 635 label for the CD31 antibody (635 nm), the newly formed xylenol-stained bone is also evident in Figure 8D. However, only CD31 and endomucin were evident in the newly formed bone near the blood vessels in the center of the canal. These observations are consistent with a previous study evaluating monophasic apatite cements implanted in tibial plateau defects in dogs, where blood vessels and Haversian systems were observed at 32 weeks.[19]

## Histomorphometric analysis

In order to compare the rates of new bone formation and graft resorption at mechanically loaded and mechanically protected sites, histomorphometric analysis was conducted (Figure 9). Three out of four samples from each tibial plateau group were analyzed (Supplemental Figure 5). One of the BGCG/nHA-PEUR samples had a collapsed tibial shelf (Supplemental Figure 5H). One of the CG/nHA-PEUR samples showed a gap filled with fibrous tissue (Supplemental Figure 5D). This gap was attributed to a filling defect, since the fibrous tissue was localized near the mid-section of the distal surface of the implant, in contrast to the BGCG/nHA-PEUR grafts, which showed resorption around the entire perimeter of the implant. Furthermore, there was minimal evidence of residual CG/nHA-PEUR graft within the fibrous tissue. These two samples were excluded from the analysis to ensure that the results are representative. All eight samples from each femoral condyle group were analyzed. For the CG group, the area% bone was significantly higher in region 4 of the tibial plateau compared to the femoral condyle (Figure 9A). The area% CG (Figure 9B) and nHA-PEUR (Figure 9C) trended lower in some of the regions of the tibial plateau compared to the femoral condyle. These findings suggest that CG/nHA-PEUR grafts implanted at mechanically loaded sites remodeled faster than grafts implanted at mechanically protected sites. At both sites, the remodeling was balanced, as the resorbing graft was replaced by new bone. In contrast, for the BGCG/nHA-PEUR group, the area% bone was significantly lower in Regions −4 and 4 of the tibial plateau compared to the femoral condyle due to resorption (Figure 9D). Furthermore, the area% CG (Figure 9E) and area% nHA-PEUR (Figure 9F) were lower in the tibial plateau compared to the femoral condyle in some regions. These

findings suggest that remodeling of BGCG/nHA-PEUR implanted in the tibial plateau defect was not balanced, since resorption of both the implant and the host bone were observed.

New bone formation and graft resorption were also compared between sheep that were sacrificed early (6 – 20 days) due to tibial plateau shelf fractures and those that were sacrificed at the planned end point of 16 weeks for the CG/nHA-PEUR (Figure 10) and BGCG/nHA-PEUR (Supplemental Figure 6) groups. While the degree of mechanical loading in the animals that fractured likely differed from the animals that did not, only a minimal amount of new bone ingrowth and graft resorption would be expected at time points <3 weeks. Furthermore, the defects in the contra-lateral limbs did not experience shelf fractures. Data were reported for the distal surface (regions 1 to 4) only due to the fracture of the plateau shelf. New bone formation in the CG/nHA-PEUR group implanted in tibial plateau defects was higher in the outer region 4 at 16 weeks compared to <3 weeks (Figure 10A). In contrast, new bone formation in region 4 of the femoral condyle defects at 16 weeks was comparable to that <3 weeks (Figure 10B). The area% residual CG and nHA-PEUR in regions 3 and 4 trended lower at 16 weeks compared to <3 weeks. The differences in area% nHA-PEUR were significant in region 3 of both the tibial plateau and femoral condyle defects. These findings suggest that the CG/nHA-PEUR implants resorbed and were replaced by new bone in the tibial plateau defects over the period of 3 to 16 weeks. In contrast, BGCG/nHA-PEUR implants showed evidence of bone and graft resorption at the tibial plateau site over the period of 3 to 16 weeks (Supplemental Figure 6A).

## Dynamic histomorphometry

Sheep received calcein green (4 weeks), xylenol orange (8 weeks), and oxytetracycline (15 weeks) injections. Representative fluorescent images of CG/nHA-PEUR grafts implanted in tibial plateau (Figure 11A) and femoral condyle (Figure 11B) defects showed evidence of new bone stained with xylenol orange (red) and oxytetracycline (yellow-green) in the trabecular bone adjacent to the graft at 16 weeks. Representative images near the implant/bone interface (Figure 11C) show appositional new bone formation parallel to the implant surface (yellow arrows), which is consistent with appositional bone growth observed in the histological sections (Figures 6 and **7**) and trabecular thickening of host bone near the implant/bone interface observed by μCT (Figure 2F–H). Ingrowth of new bone (white arrows) stained with xylenol orange and oxytetracycline normal to the surface of CG/nHA-PEUR implanted in a femoral condyle defect was also observed. This observation is consistent with the histological images at 16 weeks (Figure 7E–F) showing that new bone formed within the implant after resorption of nHA-PEUR, since the presence of the low porosity implant precludes bone ingrowth prior to resorption of the nHA-PEUR component.

## Sclerostin expression

The Wnt signaling antagonist sclerostin is secreted by osteocytes and inhibits bone formation by osteoblasts.[43–45] Considering that mechanical stimulation reduces sclerostin expression [46], we assessed sclerostin expression at the tibial plateau and femoral condyle sites treated with CG/nHA-PEUR by IHC. Positive staining for sclerostin was observed at both anatomic sites (yellow arrows Figure 12A–B). The area% sclerostin (area stained positive for sclerostin divided by the total area) in the host bone was calculated in the region

extending from the host bone-implant interface (excluding residual implant) to 3.5 mm away from the defect. A representative area of interest at 4x magnification is shown in Figure 12C (the voids between trabeculae and the bony surfaces enclosed by the dashed yellow lines were excluded from the analysis to minimize artefacts). Host bone adjacent to the femoral condyle defects showed significantly higher expression of sclerostin compared to the tibial plateau defects (Figure 12D).

## Discussion

Repair of tibial plateau fractures often requires extensive mechanical fixation with protected weight-bearing for 10 weeks, as currently available bone grafts have inadequate mechanical properties to stabilize the defect. CPCs have initial compressive strength exceeding that of trabecular bone, but the bending strength, torsional strength, fatigue resistance, and fracture toughness are lower than that of trabecular bone[47]. Consequently, CPCs are indicated for use as a bone void filler and not for structural repair of bone[20]. The objective of this study was to test the hypothesis that a resorbable bone cement with initial mechanical properties sufficiently high to support structural repair of bone (70 – 90 MPa) would stabilize mechanically loaded tibial plateau defects while actively remodeling in a large animal model. Implantation of the cements in mechanically protected femoral condyle defects allowed for investigation of the effects of loading on remodeling. The initial compressive strengths of the cements exceeded 75 MPa. The cements also showed a fatigue life of >1,000,000 cycles at a physiological loading of 5 MPa[48], compared to 23,500 cycles for a biphasic CPC[26]. When implanted in mechanically loaded tibial plateau defects without external fixation, CG/nHA-PEUR cements stabilized the defect for 16 weeks and showed evidence of cellular infiltration, new bone formation, osteoclast-mediated resorption, and integration with host bone.

While hydroxyapatite and β-tricalcium phosphate undergo solution-mediated dissolution, they have relatively low solubility and remodel primarily by creeping substitution, a process characterized by an appositional bone formation phase followed by a resorptive phase[49]. In contrast, 45S5 bioactive glass (BG) more readily dissolves to release ionic species that stimulate new bone formation.[50–54] We blended BG with CG in the BGCG/nHA-PEUR group to test the hypothesis that the BG particles would accelerate remodeling of the composite cements. In tibial plateau defects, BGCG/nHA-PEUR cements almost completely resorbed by 16 weeks, resulting in formation of a dense rim of cortical bone surrounding the defect. However, BGCG/nHA-PEUR cements implanted in femoral condyle defects showed balanced new bone formation and graft resorption with minimal fibrous tissue after 16 weeks. In a previous study, composites consisting of 60% polyurethane and 40% calcium silicophosphate glass granules (63 – 200 μm) remained intact for 24 months after implantation and showed ingrowth of new bone when implanted in mechanically loaded tibial plateau defects in sheep[55]. However, this model was less mechanically stringent than that used in the present study due to the fact that the cortex was not removed, as evidenced by the observation that empty defects remained stable throughout the study[56]. Considering that BGCG/nHA-PEUR was stable in the femoral plug defects and exhibited comparable initial mechanical properties to CG/nHA-PEUR, the extensive resorption observed in the

tibial plateau defects is likely related to a combination of mechanical loading and cellular interactions with the graft.

The nHA component enhanced both the mechanical and osteogenic properties of the cements. Since nHA-PEUR is a tacky polymer that cannot be handled prior to cure, CG or BGCG was added to yield a putty-like material that hardened in < 5 min, which is comparable to working times for CPCs.[47] Addition of CG or BGCG reduced the ultimate compressive strength of the composites to 82 – 92 MPa (Figure 1C) compared to nHA-PEUR hybrid polymers alone (100 MPa [29]). However, while the addition of the granules reduced the initial compressive strength of the cements, it remained within the range of bone cements indicated for structural repair of bone (70 – 90 MPa).[57] Previous studies have shown that nHA with grain size less than 100 nm enhances osteogenic differentiation compared to micron-scale HA.[58–66] We have recently reported that human mesenchymal stem cells (hMSCs) cultured on nHA-PEUR promoted osteogenic differentiation and osteoid mineralization within 7 days, compared to 21 days for PEUR without nHA[29, 67]. Histological sections of CG/nHA-PEUR cements at 16 weeks showed minimal evidence of fibrous tissue, in contrast to previous studies with PEUR bone cements, which showed a greater degree of infiltration with fibroblasts and fibrous tissue[37, 68]. These previous studies support the notion that the nHA component of the polymer stimulated new bone formation, resulting in minimal ingrowth of fibrous tissue.

Both histology (Figure 7A–B) and dynamic histomorphometry (yellow arrows, Figure 11C) images showed evidence of appositional new bone formation near the bone/implant interface, which is consistent with trabecular thickening of the bone near the interface observed by μCT (Figure 2F–H). Histology (Figure 7E–F) and dynamic histomorphometry (white arrows, Figure 11C) images at 16 weeks show that new bone grew into the implants through newly formed pores resulting from resorption of the nHA-PEUR component. This remodeling pattern is consistent with our previous finding that nHA-PEUR supports osteoclast-mediated resorption (due to the presence of nHA) both *in vitro*[29] and *in vivo*[30]. In addition, the PEUR component undergoes oxidative degradation of the lysine residue in the polymer[33]. Trabecular thickening of host bone adjacent to the implant and ingrowth of new bone into the implant suggest that mechanical loading is adequately transferred through the implant to the bone at 16 weeks. A previous study evaluating a biphasic CPC consisting of dicalcium phosphate dehydrate (DCPD) and β-TCP granules also showed ingrowth of new bone similar to that observed for CG/nHA-PEUR. Due to its faster degradation rate, the DCPD component was resorbed first, resulting in incorporation of free β-TCP granules within new bone[20, 69–71]. Other biphasic CPCs reinforced with polymers or metals show enhanced mechanical properties[36, 72–74] but have not been evaluated in mechanically loaded defect models.

Differences in graft remodeling were observed between the mechanically loaded and mechanically protected defects. In region 4 (Figure 9), 40 area% bone was observed in the tibial plateau defects, which was significantly higher than that measured in the femoral condyle defects (24 area%). Similarly, the area% CG in regions 3 and 4 of the tibial plateau defect trended lower than that in the femoral condyle defect. While the differences in surface curvature between the tibial slab-like and femoral cylindrical defects may limit comparison

of the two anatomic sites, the radius of curvature of the femoral defects (4 mm) is at least an order of magnitude larger than the thickness of the trabeculae (<300 μm, Figure 2H). Other limitations to the histomorphometry approach include the challenges of dividing the implants into eight 1-mm thick regions and the mixed (bone and residual graft) composition of the outermost region. However, in a similar study assessing allograft bone composites implanted in 6-mm femoral condyle defects in rabbits, we also observed an increase in area % bone in the outermost 1-mm thick region compared to the internal regions at 12 weeks[37]. Furthermore, our histomorphometic findings are consistent with the trabecular thickening of bone adjacent to the implant compared to that far from the implant assessed by μCT (Figure 2F–H).

Wnt signaling through the transmembrane low-density lipoprotein receptor Lrp5 is required for mechanical loading to initiate bone formation[75]. Sclerostin is secreted by osteocytes and inhibits Wnt signaling by binding to Lrp5[43]. When osteocytes sense mechanical stimuli, they reduce the production of sclerostin (encoded by SOST), which activates osteoblasts to stimulate new bone formation[75, 76]. Interestingly, expression of sclerostin was approximately 2.4 times higher in the femoral condyle compared to the tibial plateau (Figure 12C). This finding is consistent with a previous study reporting that mechanical loading reduces sclerostin expression[46]. Thus, decreased sclerostin expression in mechanically loaded grafts may contribute to their faster remodeling compared to mechanically protected grafts. Additional studies are warranted to fully elucidate the relative contribution of sclerostin to remodeling of bone grafts under mechanical loading.

Previous studies in mechanically protected defects have reported that calcium phosphate and HA cements remodel faster at femoral sites due to increased cell density and blood flow compared to the tibia[71, 77]. These findings suggest that in the canine model, where the rates of new bone formation were similar for tibial plateau and femoral plug defects[19], the effects of higher mechanical loading at the tibial plateau offset the effects of increased cell density and blood flow at the femoral condyle, resulting in comparable remodeling between the two sites. However, in larger animals such as sheep the effects of mechanical loading have been reported to enhance remodeling. In a previous study, a ceramic coating improved osseointegration of alumina in a mechanically loaded defect but not in a mechanically protected drill hole in sheep tibiae[78]. A controlled loading experiment further indicated that mechanical stimuli associated with physiological stresses improved incorporation and remodeling of morselized bone graft in goat femurs[79]. Taken together, these findings suggest that the increased mechanical loading in the sheep tibial plateau defects stimulated new bone formation and CG/nHA-PEUR graft resorption compared to the femoral plug defects[71].

While the tibial plateau slot defect is a mechanically stringent model of bone regeneration, there are limitations to the model. Remodeling of the grafts was evaluated at a single 4-month time point, which is an established time point for evaluation of bone healing in sheep[20, 68]. Evaluation of remodeling at longer time points in future studies is necessary to ensure that the grafts maintain mechanical stability throughout the duration of the healing process[68]. Among the four (two CG/nHA-PEUR and two BGCG/nHA-PEUR) tibial plateau defects that fractured at early time points (6 – 20 days), three fractured on the

posterior side of the tibial shelf, which has been reported to be the weakest site due to a discontinuity in the bone architecture[79]. Micro-motion of the tibial shelf caused by mechanical loading and consequent pull-up strain by the anterior cruciate ligament (ACL) prior to sufficient integration of the graft with host bone is a potential cause of the fractures, which were not observed in the mechanically protected femoral condyle defects. However, it was not possible to determine which occurred first, the rupture of the patellar tendon or the fracture of the shelf. The animals were kept in a sling system for only 3 days before they were allowed to return to normal weight-bearing activities, which is shorter than the 14-day period reported previously[20]. Taken together, these observations suggest that a minimum period of reduced weight-bearing of 2 – 4 weeks may be necessary to allow for sufficient integration of the graft with host bone.

For the first time, we report a resorbable bone cement that stabilized mechanically loaded defects and remodeled to form new bone in a stringent weight-bearing model in sheep. We also found that a resorbable bone graft (BGCG/nHA-PEUR) that is stable in mechanically protected femoral condyle defects showed excessive resorption and cracking in the mechanically loaded tibial plateau defects. These findings underscore the importance of testing cements designed for structural repair of bone in stringent models of weight-bearing fractures.

## Conclusions

Resorbable ceramic granule CG/nHA-PEUR bone cements with initial mechanical properties potentially suitable for structural repair of bone remodeled to form new bone while maintaining mechanical stability in a stringent weight-bearing tibial plateau defect model in sheep. The rate of remodeling of the cement was significantly faster at mechanically loaded tibial defects compared to mechanically protected femoral defects. CG/nHA-PEUR cements exhibited handling properties comparable to conventional bone cements, stimulated new bone formation, supported osteoclast-mediated resorption, and integrated with host bone at 16 weeks. These findings highlight the potential of these materials as resorbable, weight-bearing bone cements.

## Supplementary Material

Refer to Web version on PubMed Central for supplementary material.

## Acknowledgments

Research reported in this publication was supported by the National Institute of Arthritis and Musculoskeletal and Skin Diseases of the National Institutes of Health under Award Number R01 AR064304. Madison McGough was supported by an NSF Graduate Student Research Fellowship. Confocal images of sheep immunofluorescence staining were obtained through the use of the Vanderbilt Cell Imaging Shared Resource, supported by NIH grants CA68485, DK20593, DK59637, DK58404 and EY08126. The content is solely the responsibility of the authors and does not necessarily represent the official views of the National Institutes of Health or the National Science Foundation.

## References


1. Anderson DD, Van Hofwegen C, Marsh JL, Brown TD. Is elevated contact stress predictive of post-traumatic osteoarthritis for imprecisely reduced tibial plafond fractures? J Orthop Res. 2011; 29(1): 33–9. [PubMed: 20607840]
2. Goff T, Kanakaris NK, Giannoudis PV. Use of bone graft substitutes in the management of tibial plateau fractures. Injury-International Journal of the Care of the Injured. 2013; 44:S86–S94.
3. Simpson D, Keating JF. Outcome of tibial plateau fractures managed with calcium phosphate cement. Injury. 2004; 35(9):913–8. [PubMed: 15302246]
4. Hall JA, Beuerlein MJ, McKee MD. Open reduction and internal fixation compared with circular fixator application for bicondylar tibial plateau fractures. Surgical technique. J Bone Joint Surg Am. 2009; 91(Suppl 2 Pt 1):74–88.
5. Ali AM, El-Shafie M, Willett KM. Failure of fixation of tibial plateau fractures. J Orthop Trauma. 2002; 16(5):323–9. [PubMed: 11972075]
6. Bosse MJ, MacKenzie EJ, Kellam JF, Burgess AR, Webb LX, Swiontkowski MF, Sanders RW, Jones AL, McAndrew MP, Patterson BM, McCarthy ML, Travison TG, Castillo RC. An analysis of outcomes of reconstruction or amputation after leg-threatening injuries. N Engl J Med. 2002; 347(24):1924–31. [PubMed: 12477942]
7. Aamodt A, Nordsletten L, Havelin LI, Indrekvam K, Utvag SE, Hviding K. Documentation of hip prostheses used in Norway - A critical review of the literature from 1996–2000. Acta Orthopaedica Scandinavica. 2004; 75(6):663–676. [PubMed: 15762255]
8. Berry DJ, Harmsen WS, Cabanela ME, Morrey BF. Twenty-five-year survivorship of two thousand consecutive primary Charnley total hip replacements - Factors affecting survivorship of acetabular and femoral components. Journal of Bone and Joint Surgery-American Volume. 2002; 84A(2):171–177.
9. Bettencourt A, Calado A, Amaral J, Alfaia A, Vale FM, Monteiro J, Montemor MF, Ferreira MGS, Castro M. Surface studies on acrylic bone cement. International Journal of Pharmaceutics. 2004; 278(1):181–186. [PubMed: 15158960]
10. Jasty M, Maloney WJ, Bragdon CR, Oconnor DO, Haire T, Harris WH. THE INITIATION OF FAILURE IN CEMENTED FEMORAL COMPONENTS OF HIP ARTHROPLASTIES. Journal of Bone and Joint Surgery-British Volume. 1991; 73(4):551–558.
11. Savarino L, Stea S, Ciapetti G, Paganetto G, Donati ME, Alvergna P, Pizzoferrato A. MICROSTRUCTURAL INVESTIGATION OF BONE-CEMENT INTERFACE. Journal of Biomedical Materials Research. 1995; 29(6):701–705. [PubMed: 7593006]
12. Bhaskar SN, Brady JM, Getter L, Grower MF, Driskell T. BIODEGRADABLE CERAMIC IMPLANTS IN BONE - ELECTRON AND LIGHT MICROSCOPIC ANALYSIS. Oral Surgery Oral Medicine Oral Pathology Oral Radiology and Endodontics. 1971; 32(2):336.
13. Cameron HU, Macnab I, Pilliar RM. EVALUATION OF A BIODEGRADABLE CERAMIC. Journal of Biomedical Materials Research. 1977; 11(2):179–186. [PubMed: 853042]
14. Constantz BR, Ison IC, Fulmer MT, Poser RD, Smith ST, Vanwagoner M, Ross J, Goldstein SA, Jupiter JB, Rosenthal DI. SKELETAL REPAIR BY IN-SITU FORMATION OF THE MINERAL PHASE OF BONE. Science. 1995; 267(5205):1796–1799. [PubMed: 7892603]
15. HubbardW. Physiological calcium phosphates as orthopaedic biomaterialsMarquette University; Milwaukee, Wisconsin: 1974
16. ManleyMT. Calcium phosphate biomaterials. A review of the literature. In: GeesinkRGT, , ManleyMT, editorsHydroxylapatite coatings in orthopaedic surgeryRaven Press; New York: 1993123
17. Moore DC, Chapman MW, Manske D. THE EVALUATION OF A BIPHASIC CALCIUM-PHOSPHATE CERAMIC FOR USE IN GRAFTING LONG-BONE DIAPHYSEAL DEFECTS. Journal of Orthopaedic Research. 1987; 5(3):356–365. [PubMed: 3040949]
18. Nelson DGA. THE INFLUENCE OF CARBONATE ON THE ATOMIC-STRUCTURE AND REACTIVITY OF HYDROXYAPATITE. Journal of Dental Research. 1981; 60:1621–1629. [PubMed: 6943172]

19. Frankenburg EP, Goldstein SA, Bauer TW, Harris SA, Poser RD. Biomechanical and histological evaluation of a calcium phosphate cement. Journal of Bone and Joint Surgery-American Volume. 1998; 80A(8):1112–1124.
20. Gisep A, Wieling R, Bohner M, Matter S, Schneider E, Rahn B. Resorption patterns of calcium-phosphate cements in bone. Journal of Biomedical Materials Research Part A. 2003; 66A(3):532–540.
21. Bennett S, Connolly K, Lee DR, Jiang Y, Buck D, Hollinger JO, Gruskin EA. Initial biocompatibility studies of a novel degradable polymeric bone substitute that hardens in situ. Bone. 1996; 19(1):S101–S107.
22. Bonzani IC, Adhikari R, Houshyar S, Mayadunne R, Gunatillake P, Stevens MM. Synthesis of two-component injectable polyurethanes for bone tissue engineering. Biomaterials. 2007; 28(3):423–433. [PubMed: 16979756]
23. Dumas JE, Davis T, Holt GE, Yoshii T, Perrien DS, Nyman JS, Boyce T, Guelcher SA. Synthesis, characterization, and remodeling of weight-bearing allograft bone/polyurethane composites in the rabbit. Acta Biomaterialia. 2010; 6(7):2394–2406. [PubMed: 20109586]
24. Guelcher SA. Biodegradable polyurethanes: Synthesis and applications in regenerative medicine. Tissue Engineering Part B-Reviews. 2008; 14(1):3–17. [PubMed: 18454631]
25. Hafeman AE, Li B, Yoshii T, Zienkiewicz K, Davidson JM, Guelcher SA. Injectable biodegradable polyurethane scaffolds with release of platelet-derived growth factor for tissue repair and regeneration. Pharmaceutical Research. 2008; 25(10):2387–2399. [PubMed: 18516665]
26. Harmata AJ, Uppuganti S, Granke M, Guelcher SA, Nyman JS. Compressive fatigue and fracture toughness behavior of injectable, settable bone cements. Journal of the mechanical behavior of biomedical materials. 2015; 51:345–355. [PubMed: 26282077]
27. Johnson AJW, Herschler BA. A review of the mechanical behavior of CaP and CaP/polymer composites for applications in bone replacement and repair. Acta Biomaterialia. 2011; 7(1):16–30. [PubMed: 20655397]
28. Prieto EM, Talley AD, Gould NR, Zienkiewicz KJ, Drapeau SJ, Kalpakci KN, Guelcher SA. Effects of particle size and porosity on in vivo remodeling of settable allograft bone/polymer composites. Journal of Biomedical Materials Research Part B-Applied Biomaterials. 2015; 103(8): 1641–1651.
29. Lu S, McGough MAP, Rogers BR, Wenke JC, Shimko D, Guelcher SA. Resorbable nanocomposites with bone-like strength and enhanced cellular activity. Journal of Materials Chemistry B. 2017; 5(22):4198–4206.
30. McEnery MA, Lu S, Gupta MK, Zienkiewicz KJ, Wenke JC, Kalpakci KN, Shimko DA, Duvall CL, Guelcher SA. Oxidatively degradable poly (thioketal urethane)/ceramic composite bone cements with bone-like strength. RSC advances. 2016; 6(111):109414–109424. [PubMed: 27895899]
31. Guelcher SA, Srinivasan A, Dumas JE, Didier JE, McBride S, Hollinger JO. Synthesis, mechanical properties, biocompatibility, and biodegradation of polyurethane networks from lysine polyisocyanates. Biomaterials. 2008; 29(12):1762–1775. [PubMed: 18255140]
32. Lu S, McGough M, Rogers B, Wenke J, Shimko D, Guelcher S. Resorbable nanocomposites with bone-like strength and enhanced cellular activity. Journal of Materials Chemistry B. 2017; 5(22): 4198–4206.
33. Hafeman AE, Zienkiewicz KJ, Zachman AL, Sung HJ, Nanney LB, Davidson JM, Guelcher SA. Characterization of the degradation mechanisms of lysine-derived aliphatic poly(ester urethane) scaffolds. Biomaterials. 2011; 32(2):419–429. [PubMed: 20864156]
34. Harmata AJ, Ward CL, Zienkiewicz KJ, Wenke JC, Guelcher SA. Investigating the effects of surface-initiated polymerization of e-caprolactone to bioactive glass particles on the mechanical properties of settable polymer/ceramic composites. Journal of Materials Research. 2014; 29(20): 2398–2407. [PubMed: 25798027]
35. Harmata AJ, Ward CL, Zienkiewicz KJ, Wenke JC, Guelcher SA. Investigating the effects of surface-initiated polymerization of epsilon-caprolactone to bioactive glass particles on the mechanical properties of settable polymer/ceramic composites. Journal of Materials Research. 2014; 29(20):2398–2407. [PubMed: 25798027]

36. Dumas JE, Zienkiewicz K, Tanner SA, Prieto EM, Bhattacharyya S, Guelcher SA. Synthesis and Characterization of an Injectable Allograft Bone/Polymer Composite Bone Void Filler with Tunable Mechanical Properties. Tissue Engineering Part A. 2010; 16(8):2505–2518. [PubMed: 20218874]
37. Dumas JE, Prieto EM, Zienkiewicz KJ, Guda T, Wenke JC, Bible J, Holt GE, Guelcher SA. Balancing the Rates of New Bone Formation and Polymer Degradation Enhances Healing of Weight-Bearing Allograft/Polyurethane Composites in Rabbit Femoral Defects. Tissue Engineering Part A. 2014; 20(1–2):115–129. [PubMed: 23941405]
38. Wolfram U, Schwiedrzik J. Post-yield and failure properties of cortical bone. BoneKEy reports. 2016; 5
39. Pobloth AM, Johnson KA, Schell H, Kolarczik N, Wulsten D, Duda GN, Schmidt-Bleek K. Establishment of a preclinical ovine screening model for the investigation of bone tissue engineering strategies in cancellous and cortical bone defects. BMC musculoskeletal disorders. 2016; 17(1):111. [PubMed: 26932531]
40. Gisep A, Kugler S, Wahl D, Rahn B. Mechanical characterisation of a bone defect model filled with ceramic cements. J Mater Sci: Mater Med. 2004; 15(10):1065–1071. [PubMed: 15516866]
41. Talley AD, McEnery MA, Kalpakci KN, Zienkiewicz KJ, Shimko DA, Guelcher SA. Remodeling of injectable, low-viscosity polymer/ceramic bone grafts in a sheep femoral defect model. Journal of Biomedical Materials Research Part B: Applied Biomaterials. 2016
42. van Gaalen SM, Kruyt MC, Geuze RE, de Bruijn JD, Alblas J, Dhert WJ. Use of fluorochrome labels in in vivo bone tissue engineering research. Tissue engineering Part B: Reviews. 2010; 16(2):209–217. [PubMed: 19857045]
43. Robling AG, Castillo AB, Turner CH. Biomechanical and molecular regulation of bone remodeling. Annu Rev Biomed Eng. 2006; 8:455–498. [PubMed: 16834564]
44. Turner CH, Warden SJ, Bellido T, Plotkin LI, Kumar N, Jasiuk I, Danzig J, Robling AG. Mechanobiology of the skeleton. Science signaling. 2009; 2(68):pt3. [PubMed: 19401590]
45. Van Bezooijen RL, Roelen BA, Visser A, Van Der Wee-pals L, De Wilt E, Karperien M, Hamersma H, Papapoulos SE, Ten Dijke P, Löwik CW. Sclerostin is an osteocyte-expressed negative regulator of bone formation, but not a classical BMP antagonist. Journal of Experimental Medicine. 2004; 199(6):805–814. [PubMed: 15024046]
46. Tu X, Rhee Y, Condon KW, Bivi N, Allen MR, Dwyer D, Stolina M, Turner CH, Robling AG, Plotkin LI. Sost downregulation and local Wnt signaling are required for the osteogenic response to mechanical loading. Bone. 2012; 50(1):209–217. [PubMed: 22075208]
47. Bohner M. DESIGN OF CERAMIC-BASED CEMENTS AND PUTTIES FOR BONE GRAFT SUBSTITUTION. European Cells & Materials. 2010; 20:1–12. [PubMed: 20574942]
48. Ramakrishna S, Mayer J, Wintermantel E, Leong KW. Biomedical applications of polymer-composite materials: a review. Composites Science and Technology. 2001; 61(9):1189–1224.
49. Burchardt H. THE BIOLOGY OF BONE-GRAFT REPAIR. Clinical Orthopaedics and Related Research. 1983; (174):28–42.
50. Hoppe A, Guldal NS, Boccaccini AR. A review of the biological response to ionic dissolution products from bioactive glasses and glass-ceramics. Biomaterials. 2011; 32(11):2757–2774. [PubMed: 21292319]
51. Jones JR. Review of bioactive glass: From Hench to hybrids. Acta Biomaterialia. 2013; 9(1):4457–4486. [PubMed: 22922331]
52. Oonishi H, Hench LL, Wilson J, Sugihara F, Tsuji E, Matsuura M, Kin S, Yamamoto T, Mizokawa S. Quantitative comparison of bone growth behavior in granules of Bioglass (R), A-W glass-ceramic, and hydroxyapatite. Journal of Biomedical Materials Research. 2000; 51(1):37–46. [PubMed: 10813743]
53. Talley AD, Kalpakci KN, Shimko DA, Zienkiewicz KJ, Cochran DL, Guelcher SA. Effects of Recombinant Human Bone Morphogenetic Protein-2 Dose and Ceramic Composition on New Bone Formation and Space Maintenance in a Canine Mandibular Ridge Saddle Defect Model. Tissue Engineering Part A. 2016; 22(5–6):469–479. [PubMed: 26800574]

54. Franks K, Abrahams I, Knowles J. Development of soluble glasses for biomedical use Part I: In vitro solubility measurement. J Mater Sci: Mater Med. 2000; 11(10):609–614. [PubMed: 15348084]
55. Ignatius A, Unterricker K, Wenger K, Richter M, Claes L, Lohse P, Hirst H. A new composite made of polyurethane and glass ceramic in a loaded implant model: a biomechanical and histological analysis. Journal of Materials Science-Materials in Medicine. 1997; 8(12):753–756. [PubMed: 15348785]
56. Harms C, Helms K, Taschner T, Stratos I, Ignatius A, Gerber T, Lenz S, Rammelt S, Vollmar B, Mittlmeier T. Osteogenic capacity of nanocrystalline bone cement in a weight-bearing defect at the ovine tibial metaphysis. International Journal of Nanomedicine. 2012; 7:2883–2889. [PubMed: 22745551]
57. KuehnK-D. Bone CementsSpringer; Berlin: 2000
58. Laurencin CT, Kumbar SG, Nukavarapu SP. Nanotechnology and orthopedics: a personal perspective. Wiley Interdisciplinary Reviews-Nanomedicine and Nanobiotechnology. 2009; 1(1): 6–10. [PubMed: 20049774]
59. MacMillan AK, Lamberti FV, Moulton JN, Geilich BM, Webster TJ. Similar healthy osteoclast and osteoblast activity on nanocrystalline hydroxyapatite and nanoparticles of tri-calcium phosphate compared to natural bone. International Journal of Nanomedicine. 2014; 9:5627–5637. [PubMed: 25506216]
60. Meirelles L, Arvidsson A, Andersson M, Kjellin P, Albrektsson T, Wennerberg A. Nano hydroxyapatite structures influence early bone formation. Journal of Biomedical Materials Research Part A. 2008; 87A(2):299–307.
61. Meirelles L, Melin L, Peltola T, Kjellin P, Kangasniemi I, Currie F, Andersson M, Albrektsson T, Wennerberg A. Effect of Hydroxyapatite and Titania Nanostructures on Early In Vivo Bone Response. Clinical Implant Dentistry and Related Research. 2008; 10(4):245–254. [PubMed: 18384406]
62. Ngiam M, Liao SS, Patil AJ, Cheng ZY, Chan CK, Ramakrishna S. The fabrication of nano-hydroxyapatite on PLGA and PLGA/collagen nanofibrous composite scaffolds and their effects in osteoblastic behavior for bone tissue engineering. Bone. 2009; 45(1):4–16. [PubMed: 19358900]
63. Sato M, Webster TJ. Nanobiotechnology: implications for the future of nanotechnology in orthopedic applications. Expert Review of Medical Devices. 2004; 1(1):105–114. [PubMed: 16293014]
64. Sun F, Zhou H, Lee J. Various preparation methods of highly porous hydroxyapatite/polymer nanoscale biocomposites for bone regeneration. Acta Biomaterialia. 2011; 7(11):3813–3828. [PubMed: 21784182]
65. Tran PA, Sarin L, Hurt RH, Webster TJ. Opportunities for nanotechnology-enabled bioactive bone implants. Journal of Materials Chemistry. 2009; 19(18):2653–2659.
66. Webster TJ, Ergun C, Doremus RH, Siegel RW, Bizios R. Enhanced functions of osteoblasts on nanophase ceramics. Biomaterials. 2000; 21(17):1803–1810. [PubMed: 10905463]
67. Guo R, Lu S, Merkel AR, Sterling JA, Guelcher SA. Substrate modulus regulates osteogenic differentiation of rat mesenchymal stem cells through integrin beta 1 and BMP receptor type IA. Journal of Materials Chemistry B. 2016; 4(20):3584–3593. [PubMed: 27551426]
68. Talley AD, McEnery MA, Kalpakci KN, Zienkiewicz KJ, Shimko DA, Guelcher SA. Remodeling of injectable, low-viscosity polymer/ceramic bone grafts in a sheep femoral defect model. J Biomed Mater Res B Appl Biomater. 2016
69. Munting E, Mirtchi AA, Lemaitre J. BONE REPAIR OF DEFECTS FILLED WITH A PHOSPHOCALCIC HYDRAULIC CEMENT - AN IN-VIVO STUDY. Journal of Materials Science-Materials in Medicine. 1993; 4(3):337–344.
70. Ohura K, Bohner M, Hardouin P, Lemaitre J, Pasquier G, Flautre B. Resorption of, and bone formation from, new beta-tricalcium phosphate-monocalcium phosphate cements: An in vivo study. Journal of Biomedical Materials Research. 1996; 30(2):193–200. [PubMed: 9019484]
71. Theiss F, Apelt D, Brand BA, Kutter A, Zlinszky K, Bohner M, Matter S, Frei C, Auer JA, von Rechenberg B. Biocompatibility and resorption of a brushite calcium phosphate cement. Biomaterials. 2005; 26(21):4383–4394. [PubMed: 15701367]

72. Gay S, Arostegui S, Lemaitre J. Preparation and characterization of dense nanohydroxyapatite/PLLA composites. Materials Science & Engineering C-Biomimetic and Supramolecular Systems. 2009; 29(1):172–177.

73. Kruger R, Groll J. Fiber reinforced calcium phosphate cements -- on the way to degradable load bearing bone substitutes? Biomaterials. 2012; 33(25):5887–900. [PubMed: 22632767]

74. Kruger R, Seitz JM, Ewald A, Bach FW, Groll J. Strong and tough magnesium wire reinforced phosphate cement composites for load-bearing bone replacement. J Mech Behav Biomed Mater. 2013; 20:36–44. [PubMed: 23455162]

75. Robling AG, Niziolek PJ, Baldridge LA, Condon KW, Allen MR, Alam I, Mantila SM, Gluhak-Heinrich J, Bellido TM, Harris SE. Mechanical stimulation of bone in vivo reduces osteocyte expression of Sost/sclerostin. Journal of Biological Chemistry. 2008; 283(9):5866–5875. [PubMed: 18089564]

76. Sun Q, Choudhary S, Mannion C, Kissin Y, Zilberberg J, Lee WY. Ex vivo replication of phenotypic functions of osteocytes through biomimetic 3D bone tissue construction. Bone. 2018; 106:148–155. [PubMed: 29066313]

77. Lovati AB, Lopa S, Recordati C, Talo G, Turrisi C, Bottagisio M, Losa M, Scanziani E, Moretti M. In Vivo Bone Formation Within Engineered Hydroxyapatite Scaffolds in a Sheep Model. Calcified Tissue International. 2016; 99(2):209–223. [PubMed: 27075029]

78. Ignatius A, Peraus M, Schorlemmer S, Augat P, Burger W, Leyen S, Claes L. Osseointegration of alumina with a bioactive coating under load-bearing and unloaded conditions. Biomaterials. 2005; 26(15):2325–2332. [PubMed: 15585235]

79. Lamerigts NMP, Buma P, Huiskes R, Schreurs W, Gardeniers J, Slooff T. Incorporation of morsellized bone graft under controlled loading conditions. A new animal model in the goat. Biomaterials. 2000; 21(7):741–747. [PubMed: 10711971]

80. Gisep A, Kugler S, Wahl D, Rahn B. Mechanical characterisation of a bone defect model filled with ceramic cements. Journal of Materials Science-Materials in Medicine. 2004; 15(10):1065–1071. [PubMed: 15516866]

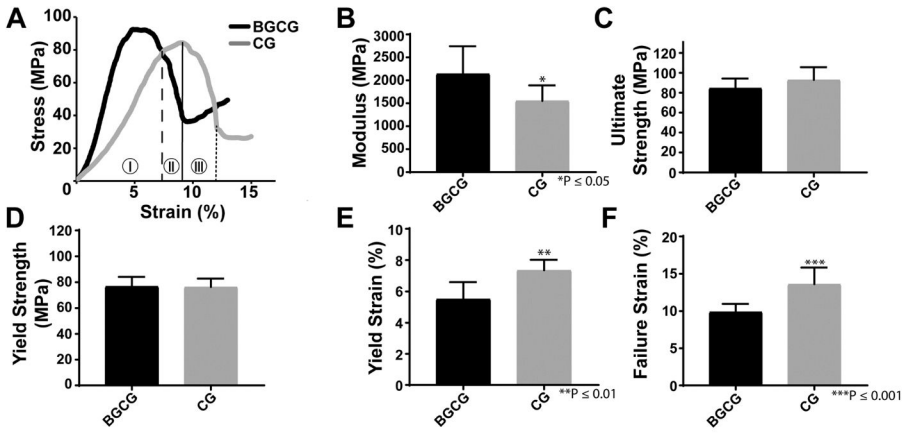


**Figure 1.**

Compression properties of the grafts cured for 24 hrs. (A) Representative stress-strain curve for the BGCG and CG groups. The vertical lines on the CG curve show points selected for yield (dashed), ultimate strength (solid), and failure (dotted) and indicate 3 zones in which the compressive properties can be analyzed: (I) elastic zone, (II) post-yield zone, and (III) fracture zone. (B) Modulus, (C) ultimate strength, (D) yield strength, (E) yield strain, and (F) failure strain were measured from the stress-strain curves. Error bars represent standard deviation. **p < 0.01, ***p<0.001.

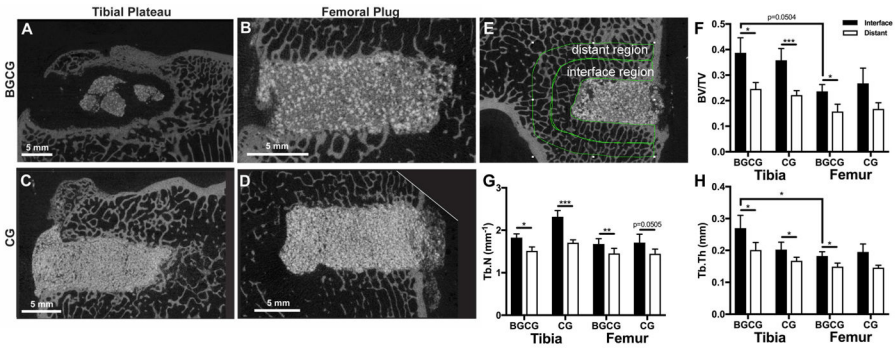


**Figure 2.**

Assessment of CG/nHA-PEUR and BGCG/nHA-PEUR implants by μCT at 16 weeks. (A – D) Representative μCT images of grafts. (A) BGCG/nHA-PEUR tibial plateau defect. (B) BGCG/nHA-PEUR femoral condyle plug defect. (C) CG/nHA-PEUR tibia plateau defect. (D) CG/nHA-PEUR femoral condyle plug defect. (E – H) μCT analysis of morphometric parameters of host bone outside the graft. (E) Representative μCT image showing the contours of the interface and distant regions used for analysis. The morphometric parameters (F) bone volume fraction (BV/TV), (G) trabecular number (Tb.N.), and (H) trabecular thickness (Tb.Th.) were calculated for all samples both the interface and distant region.

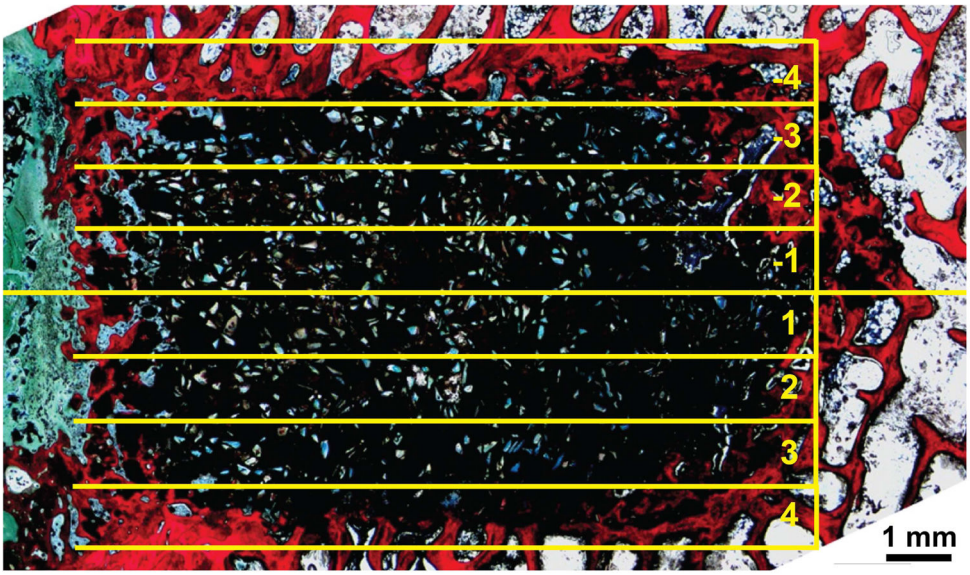


**Figure 3.**
Schematic illustrating histomorphometry areas of interest (AOI).

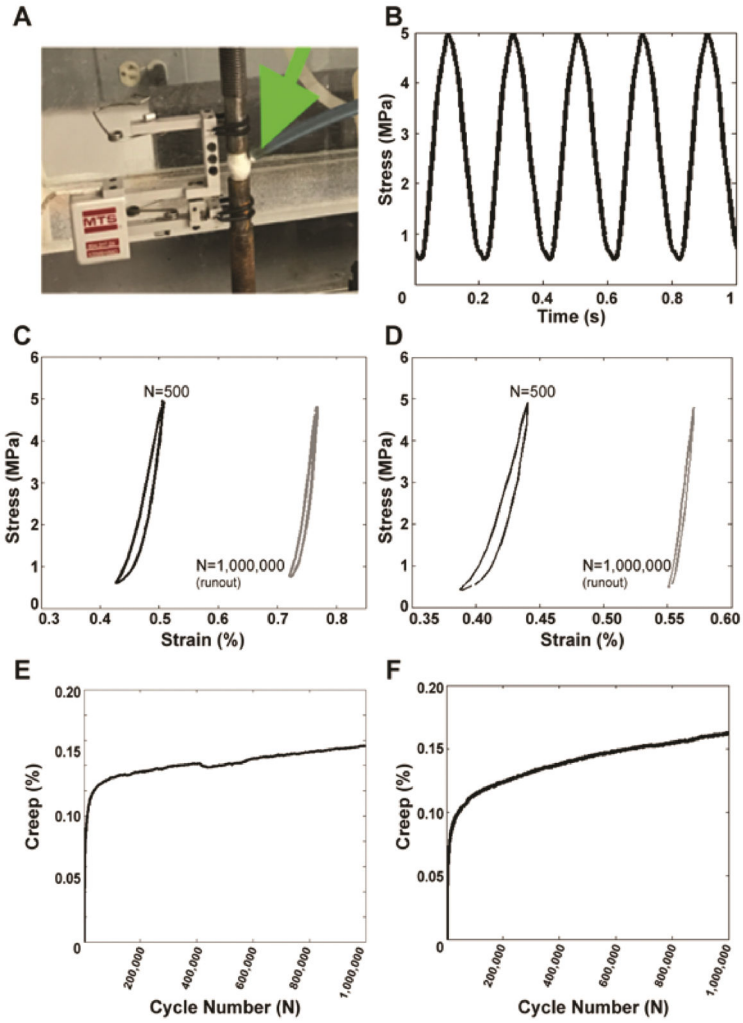


**Figure 4.**

Dynamic fatigue properties at 5 MPa applied stress. (A) Experimental setup for fatigue testing. Arrow points to water drip used to maintain hydration. (B) Samples were cyclically loaded to a maximum stress of 5 MPa (minimum ~0.3 MPa to maintain contact) at a frequency of 5 Hz. (C–D) Representative hysteresis loops for the first (black) and last (gray) recorded cycle (N= cycle number) for (C) CG/nHA-PEUR and (D) BGCG/nHA-PEUR composites. (E–F) Creep strain experienced by (E) CG/nHA-PEUR and (F) BGCG/nHA-PEUR increased dramatically the first 50,000 cycles but approached a plateau as the tests progressed.

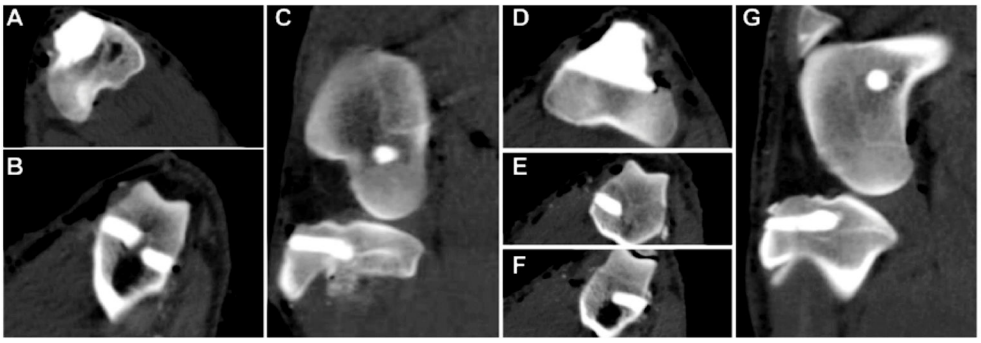


**Figure 5.**

Representative CT images of a CG/nHA-PEUR (A – C) and BGCG/nHA-PEUR (D – G) implant on the day of surgery showing fill of the defects. (A) Axial view of CG/nHA-PEUR tibial plateau defect. (B) Axial view of CG/nHA-PEUR femoral plug defects. (C) Sagittal view of CG/nHA-PEUR tibia plateau and femoral plug defects. (D) Axial view of BGCG/nHA-PEUR tibial plateau defect. (E–F) Axial view of BGCG/nHA-PEUR femoral plug defects. (G) Sagittal view of BGCG/nHA-PEUR tibia plateau and femoral plug defects.

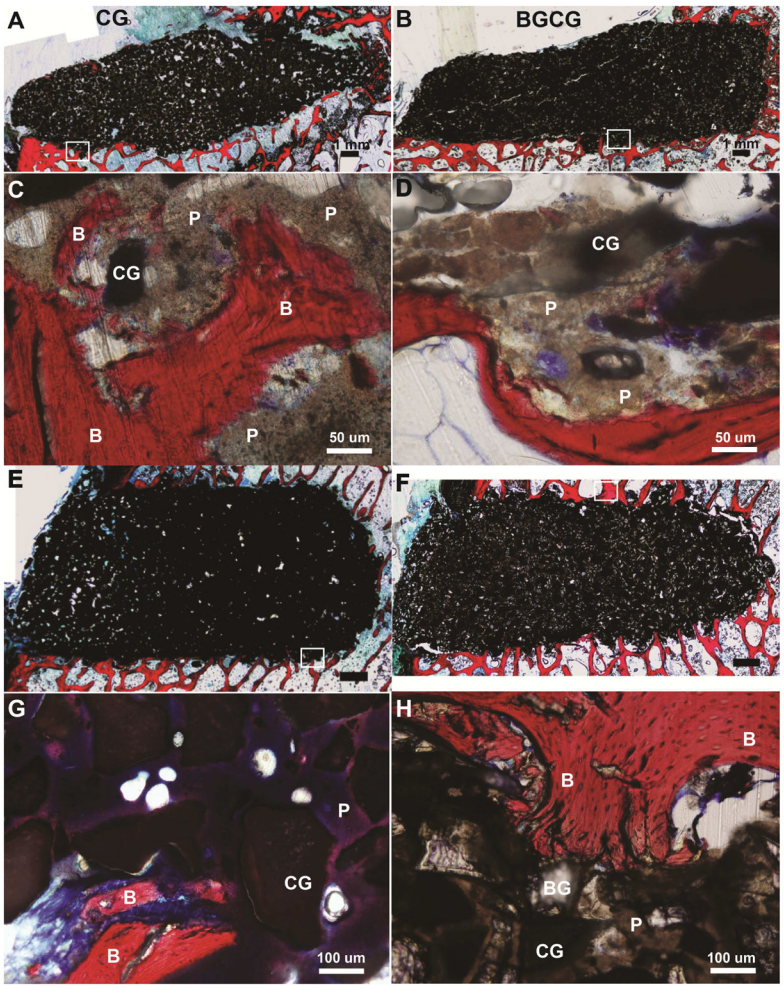


**Figure 6.**

Representative histological images of defects in sheep that were sacrificed between 6 – 20 days due to tibial plateau fractures. (A,B) Low magnification images of (A) CG/nHA-PEUR and (B) BGCG/nHA-PEUR tibial plateau defects. (C,D) High magnification images of (C) CG/nHA-PEUR and (D) BGCG/nHA-PEUR tibial plateau defects near the host bone interface. B denotes bone (stained red), P residual nHA-PEUR polymer (stained light gray), and CG residual ceramic granules (stained dark gray) (E,F) Low magnification images of (E) CG/nHA-PEUR and (F) BGCG/nHA-PEUR femoral plug defects. (G,H) High magnification images of (G) CG/nHA-PEUR and (H) BGCG/nHA-PEUR femoral plug defects near the host bone interface. BG particles appear transparent[1] and CG particles appear dark gray.[2]

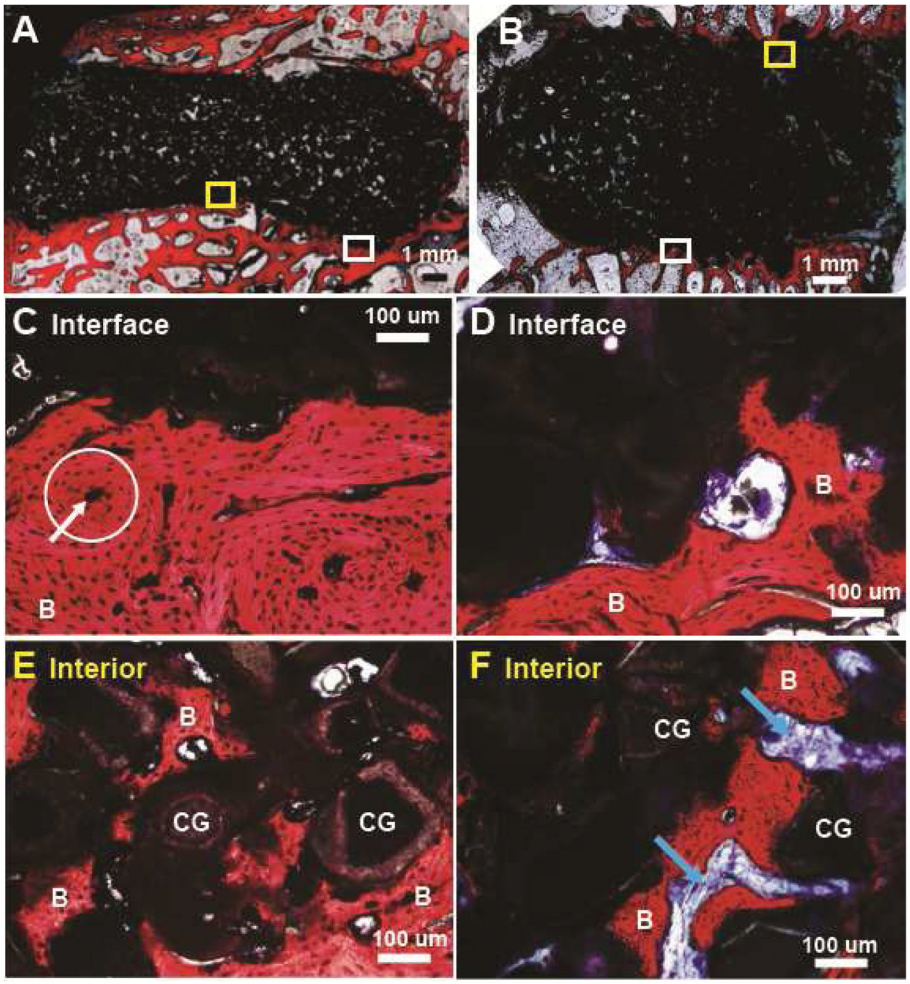


**Figure 7.**

Representative histological sections through the defects at 16 weeks. (A,C,E) Low and high magnification images of CG/nHA-PEUR tibial plateau defect at the (C) interface and (E) interior. A representative osteon is encircled (white circle) and the white arrow points to the Haversian canal. (B,D,F) Low and high magnification images of CG/nHA-PEUR femoral plug defect at the (D) interface and (F) interior. B denotes bone and CG denotes ceramic granules.

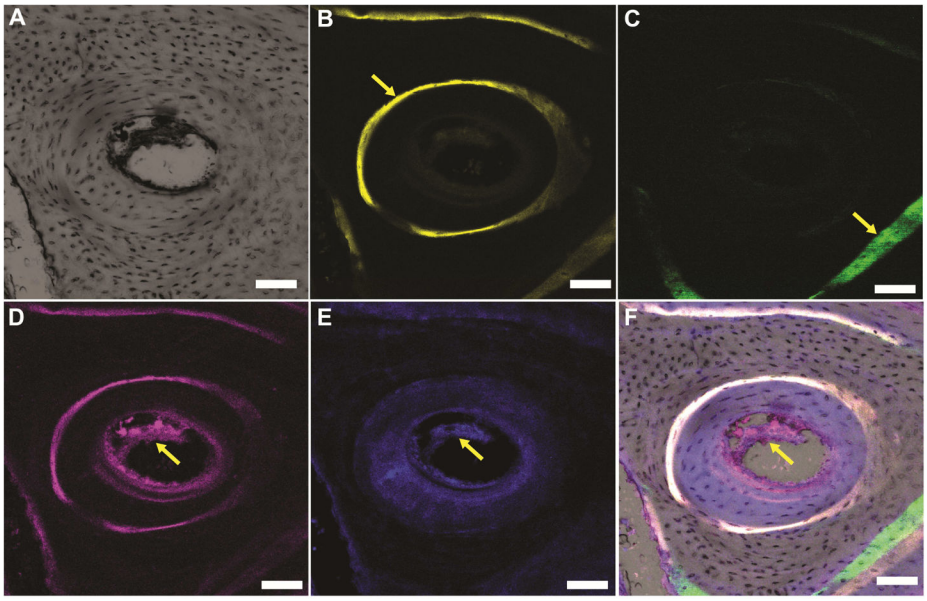


**Figure 8.**

High-magnification confocal microscope images (scale bar = 100 μm) of a representative Haversian system present in new bone formed near the CG/nHA-PEUR cement. (A) Bright-field image of a representative osteon. (B) Fluorescent image of the fluorochrome xylenol orange verifies that new bone was mineralizing to form Haversian systems at 8 weeks (yellow arrow). (C) Fluorescent image of the fluorochrome calcein green (yellow arrow) reveals evidence of new bone formation outside the osteon at 4 weeks. (D-E) Immunofluorescence staining of the endothelial markers (D) CD 31 (stained red, yellow arrow) and (E) endomucin (stained blue, yellow arrow) reveals the formation of Haversian systems. (F) Overlay of the images in Panels B – E.

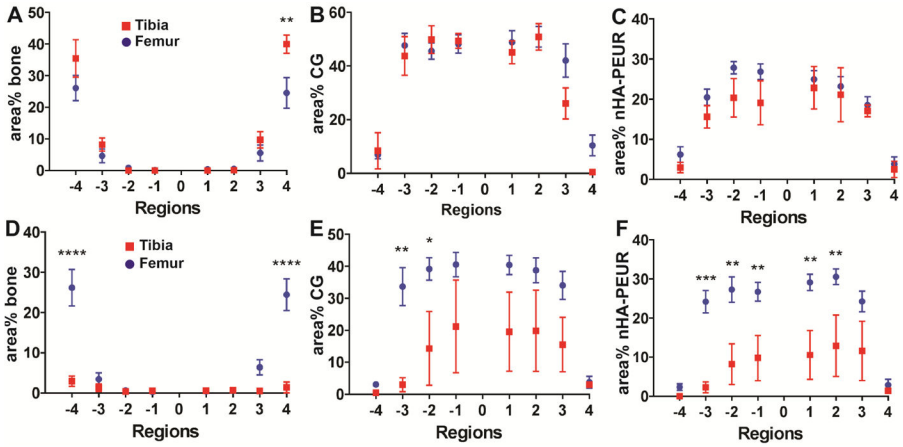


**Figure 9.**

Histomorphometric comparison of new bone formation and graft resorption between the tibial plateau and femoral condyle defects. (A) area% bone for the CG group, (B) area% CG for the CG group, (C) area% nHA-PEUR for the CG group, (D) area% bone for the BGCG group, (E) area% CG for the BGCG group, (F) area% nHA-PEUR for the BGCG group. Error bars represent SEM. Significant differences: * $p < 0.05$, ** $p < 0.01$, *** $p < 0.005$, **** $p < 0.001$.

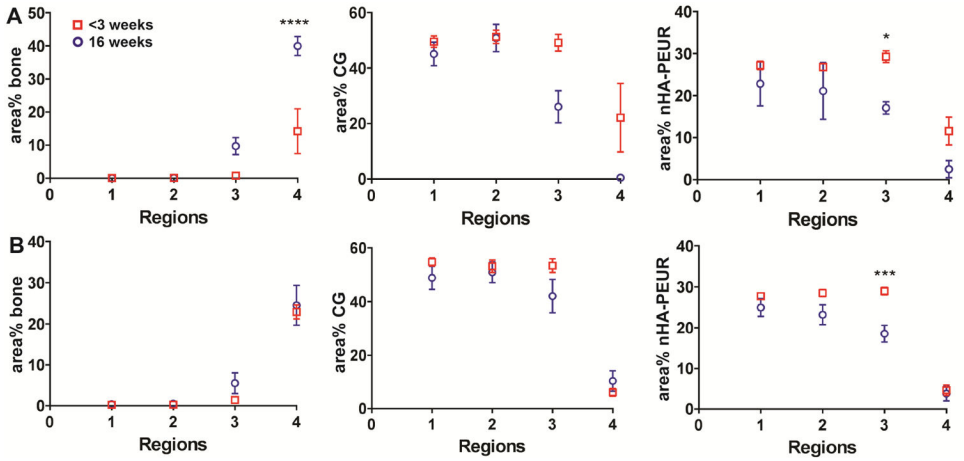


**Figure 10.**

Histomorphometric comparison of new bone formation and graft resorption between the early (<3 weeks) and late (16 weeks) time points for the CG/nHA-PEUR group. (A) Tibial plateau and (B) femoral condyle defects. Error bars represent SEM. * $p < 0.05$, *** $p < 0.005$, **** $p < 0.001$.

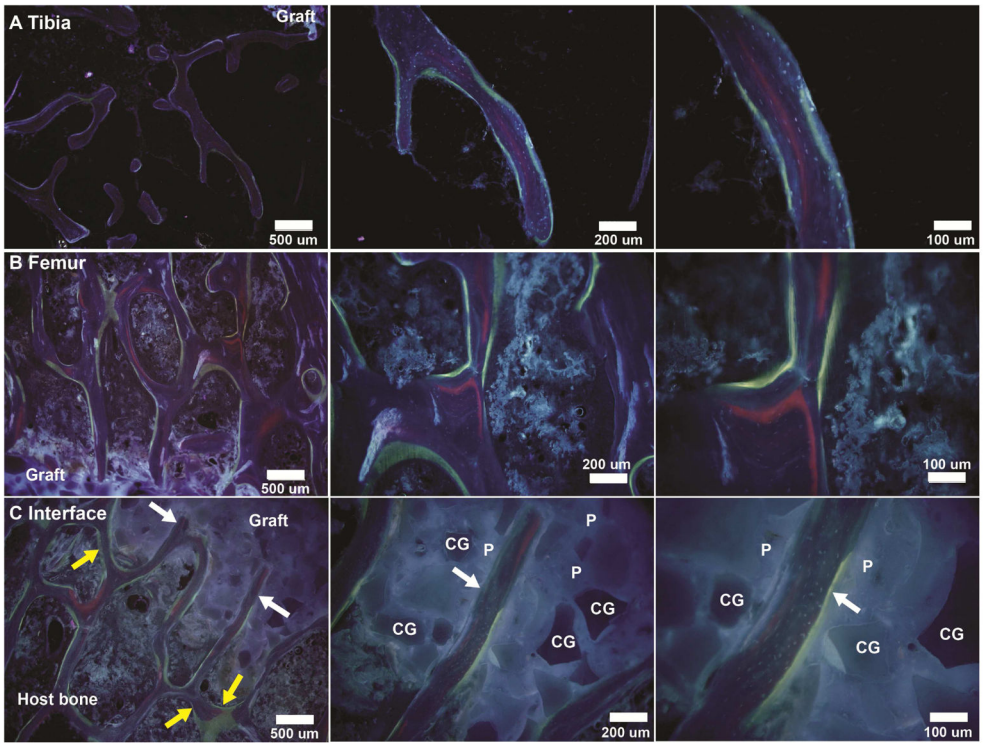


**Figure 11.**

Representative dynamic histomorphometry images of CG/nHA-PEUR grafts showing areas of xylenol orange (red, 8 weeks) and oxytetracycline (yellow-green, 15 weeks) binding. (A–B) New bone formation near the bone-graft interface in the (A) tibial plateau and (B) femoral condyle defects. (C) Appositional growth of new bone parallel to the surface (yellow arrows) and ingrowth of new bone (white arrows) into CG/nHA-PEUR grafts implanted in a femoral condyle defect. CG denotes ceramic granules and P nHA-PEUR polymer.

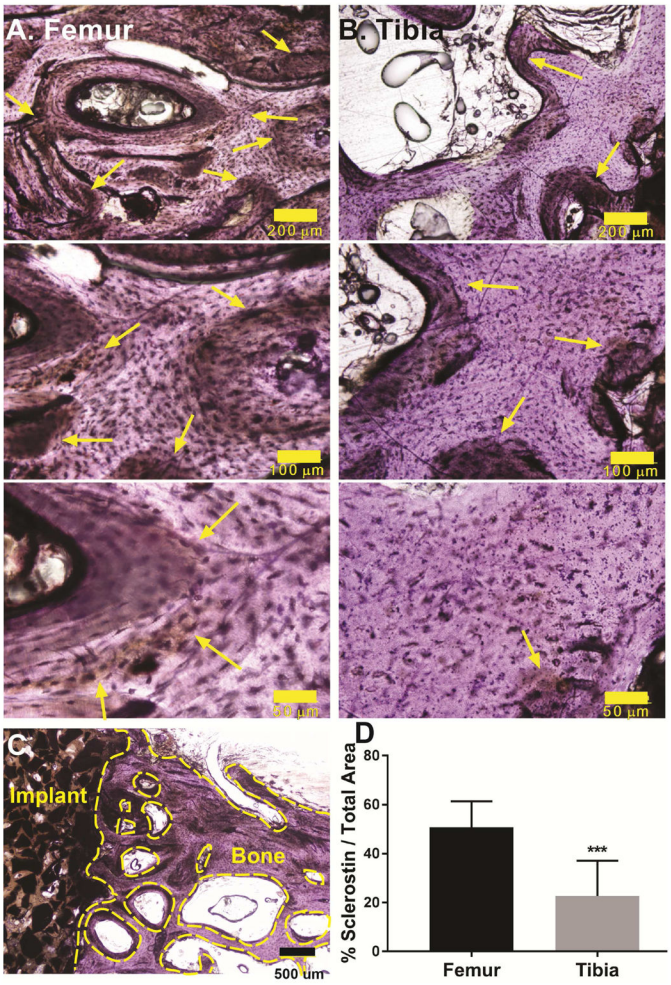


**Figure 12.**

(A–B) Representative immunohistochemical images of bone near the (A) femoral condyle and (B) tibial plateau defects at 10x (scale bar = 200 μm), 20x (scale bar = 100 μm) and 40x (scale bar = 50 μm) magnification show differential sclerostin expression (yellow arrows) in the host bone. (C) Representative area of interest in the host bone at 4x magnification (scale bar = 500 μm). The voids between trabeculae and the bony surfaces enclosed by the dashed yellow lines were excluded from the analysis to minimize artefacts. (D) Quantification of sclerostin staining of sheep femoral plug and tibial plateau defect samples reveals a significant decrease in sclerostin expression in weight-bearing tibial plateau defects. *** $p<0.0005$.

**Table 1**

Study design and handling properties of settable bone grafts.

| Treatment Group | Ceramic | Working time (min) | Tack-Free time (min) | 16 weeks | |
|---|---|---|---|---|---|
| | | | | Tibia | Femur |
| BGCG | 50 vol%BG /50 vol% CG | 2.26 ± 0.11 | 2.26 ± 0.11 | 8 | 8 |
| CG | CG | 2.08 ± 0.07 | 2.08 ± 0.07 | 8 | 8 |

**Table 2**

Compressive mechanical properties and post-yield parameters.

| | Strain at Ultimate Strength (%) **** | Post-Yield Strain (%)* | Softening (MPa) | Modulus of Resilience (MJ/m$^3$)* (zone 1) | Post-Yield Toughness (MJ/m$^3$)* (zone 2) | Fracture Zone Toughness (MJ/m$^3$)* (zone 3) | Overall Toughness (MJ/m$^3$)** (zones 1–3) | Creep at Runout (%) |
|---|---|---|---|---|---|---|---|---|
| BGCG | 6.89±0.42 | 4.39±0.45 | 54.3±5.7 | 1.71±0.14 | 1.13±0.24 | 2.20±0.28 | 5.03±0.33 | 0.14±0.02 |
| CG | 10.23±0.66 | 6.27±0.60 | 57.1±5.5 | 2.27±0.14 | 2.57±0.47 | 2.61±0.29 | 7.45±0.68 | 0.25±0.05 |

Asterisks denote statistical significance between groups:

* $p < 0.05$,

** $p < 0.01$,

**** $p < 0.001$.

**Table 3**

Preclinical outcomes of tibial plateau defects.

| Ceramic | Time to failure (days) | Radiology/necropsy observations |
|---|---|---|
| BGCG | 8 | Separation of shelf from tibia and material. Patellar tendon rupture |
| BGCG | 6 | Separation of shelf from tibia, fracture of material. Patellar tendon rupture |
| CG | 20 | Separation of shelf from material and tibia. Patellar tendon rupture |
| CG | 13 | Separation of shelf from material and tibia. Patellar tendon rupture |